IIETA International Information and Engineering Technology Association
Advancing the World of Information and Engineering

Annales de Chimie - Science des Matériaux
Vol. 50, No. 5, October, 2026, pp. 493-499
Journal homepage: http://iieta.org/journals/acsm

Investigation of Structural and Electrical Characteristics of KBT–BT Ceramics Composites

Hadeel Saad Alraheem*, Mohammed N. Al-Aaraji

Ceramic Engineering and Building Materials Department, Materials Engineering College, University of Babylon, Babylon 51001, Iraq

Corresponding Author Email: mat510.hadeel.saad@student.uobabylon.edu.iq

Copyright: ©2026 The authors. This article is published by IIETA and is licensed under the CC BY 4.0 license (http://creativecommons.org/licenses/by/4.0/).

https://doi.org/10.18280/acsm.500508

Received: 14 June 2026
Revised: 30 July 2026
Accepted: 10 August 2026
Available online: 31 October 2026

Keywords:
core-shell, dielectric properties, ferroelectric, lead-free ceramics

ABSTRACT

In the present study, a solid-state reaction was used to prepare lead-free core-shell structured ceramics (1-x)$K_{0.5}Bi_{0.5}TiO_3$ (KBT)–(x)$BaTiO_3$ (BT) (x = 0.25, 0.30 and 0.35). X-ray diffraction (XRD) analysis showed that the sintering process yielded pure perovskite phases, indicating that the heat treatment was sufficient to enable diffusion and integration of the constituent materials across all KBT compositions. The study of scanning electron microscopy (SEM) microstructure revealed that interfacial diffusion and compositional redistribution during sintering have led to distinct core-shell morphology across all KBT compositions. The sintering process enhanced the structural integrity of the samples, as indicated by good densification, and all KBT–BT ceramic samples showed comparable densities. Dielectric analysis indicates better performance of KBT–BT ceramics. The dielectric constant decreases with increasing KBT composition for the frequency range between 40 Hz and 8 MHz. On the other hand, with the rise in KBT content, the dielectric loss increases for the same range. The results show that the proposed fabrication process could be used to prepare KBT–BT ceramics with tunable core-shell microstructures and excellent functional properties. These results provide useful knowledge for the design of lead-free dielectric ceramics and open new ways for the improvement of capacitors and other electronic devices.

1. INTRODUCTION

Piezoelectric materials are of outstanding importance in modern technologies, as they have wide-ranging applications, including motors, transformers, and microelectronic components [1, 2]. Moreover, piezoelectric ceramics in commercial applications are most widely used, such as lead-zirconate titanate Pb(Zr, Ti)O_3, which contains toxic lead, thus raising health concerns and creating a dangerous environment [3, 4]. Therefore, research on lead-free piezoelectric ceramics with high performance has become an important problem [5-7].

Among the promising alternatives, $Bi_{0.5}Na_{0.5}TiO_3$ (BNT) [8], $BaTiO_3$ (BT), $K_{0.5}Na_{0.5}NbO_3$ (KNN) [9, 10], and the compound $K_{0.5}Bi_{0.5}TiO_3$ (KBT) have attracted considerable attention in recent studies, particularly when formed as a solid solution with other perovskite systems, due to their advanced dielectric and piezoelectric properties. These properties are linked to the presence of phase transition regions located near morphotropic phase boundaries (MPBs), which facilitate polarization reorientation and enhance the material's piezoelectric response [10, 11].

Recently, the formation of core-shell microstructures has received more attention as a beneficial method to accurately localise structures in lead-free ceramics. Zhang et al. [12] produced BNT and SST core-shell bars displaying improved relaxor behaviour. Xue et al. [13] efficiently minimised the temperature of sintering as well as enhanced the grain size using Li_2CO_3 addition in $Ba_{0.5}Na_{0.5}TiO_3$-$KTaO_3$ systems. Acosta et al. [14] and Ma et al. [15] utilised transmission electron microscopy (TEM), backscattered electron (BSE), and scanning electron microscopy (SEM) to detect interfaces of core-shell with distinguished contrast differences, proposing domain incoherency [16].

Sasikumar et al. [16] developed lead-free BNT-based core–shell ceramics and studied their structural and electrical properties. The modified composition improved dielectric relaxation and produced stable ferroelectric and piezoelectric performance, making it suitable for advanced piezoelectric applications.

In several recent studies [17-19], the results showed that the phase transition from the long-range ferroelectric phase to the pseudo-cubic relaxor phases was accompanied by a clear evolution in the core-shell microstructure, and this included ferroelectric areas in the core zones that were established in a relaxor ferroelectric shell. Calisir et al. [20] found that the type of ion substitution is a crucial factor that significantly affects the microstructure of the material. The isovalent and donor substitutions of La^{3+}, for Bi^{3+} and Ba^{2+} respectively, were studied in the solid solution 0.75$BiFeO_3$- 0.25BT (75BFBT). The results showed that replacing La^{3+} ions with Ba^{2+} ions at a rate of 1 mol% in 75BFBT ceramics contributed to the formation of a core-shell microstructure, where the core is a phase rich in $BiFeO_3$, while the shell is composed of a phase

rich in BT. In contrast, samples resulting from the stoichiometric substitution of Bi^{3+} ions with La^{3+} ions exhibited more homogeneous and regular microstructures, characterized by distinct and extensive piezoelectric bands across the grains. Furthermore, the application of an electric field revealed phase transitions in both the core and shell regions, reflecting the dynamic interaction of the microstructure and its response to electrical influences and its phase changes under the influence of electric polarization. Furthermore, the core retains its polarization even after the electric field is removed, while the shell is characterized by reversible phase transitions that can be recovered when the field effect is removed. Thus, the development of these core-cortical structures played an important role in achieving high and reversible electromechanical stress [21, 22]. For example, Acosta et al. [22] reported achieving an electric field-induced stress of approximately 0.3% when an electric field of 4 kV/mm was applied to BNT–$SrTiO_3$ ceramics with a core-shell microstructure. Based on these results, it was suggested that the optimal structural design of core-shell ceramics could significantly contribute to improving the material's functional properties in fatigue behaviour, hysteresis, strain output and temperature stability [23].

Barium titanate-based ceramics are primarily used in the manufacture of ceramic capacitors with high dielectric constants, as well as in lead-free piezoelectric applications. On the other hand, the use of lead-containing ceramics not only poses environmental risks and serious lead pollution but also leads to structural instability due to high lead volatilization during the sintering process [24]. KBT is a complex piezoelectric material with a perovskite structure and a relatively high Curie temperature of about 380 ℃. The (1−x)KBT–xBT system is one of the systems that has attracted a great deal of attention in scientific circles, and has been the subject of extensive studies by a large number of researchers with the aim of exploring its structural and physical properties [25, 26]. Furthermore, several studies have focused on adding KBT material to BT ceramics, given the significant effects it may have on the behavior of the positive thermal resistivity coefficient (PTCR), which contributes to improving its electrical properties and enhancing its functional performance. Some related studies and reports have also addressed the effect of adding KBT on the insulating properties of BT ceramics, particularly at high concentrations of KBT, where the results showed significant changes in the insulating behavior and electrical properties of the material [27]. The presence of polar nanoregions (PNRs) is used in characterizing these materials, as it leads to the formation of a quasi-cubic structure and the emergence of piezoelectric relaxation behavior, which has been observed in many bismuth-based perovskite systems [21, 28]. The dynamic behavior of these polar nano networks, when a material is subjected to an applied electric field that generates electrical stress, can appear as either elastic and reversible stress or inelastic and irreversible stress [23, 29]. Furthermore, the relatively low depolarization temperature, however, the significant lag in the stress-electric field curves, which in some cases exceeds 50%, as well as the need to apply high electric fields to induce the phase transition from the relaxed state to the conventional ferroelectric state, are among the most prominent challenges limiting the widespread practical application of these materials [30, 31].

Therefore, the present study aims to investigate the core–shell structures formation in KBT–BT composite ceramics fabricated via the solid-state reaction process. The study focuses on the impact of compositional variation on microstructural evolution and its correlation with dielectric properties. This work is expected to provide new insights into the role of core–shell engineering in enhancing the performance of lead-free ferroelectric ceramics and contributing to the evolution of advanced functional materials for electronic applications.

2. EXPERIMENTAL SECTION

The ceramic samples of (1-x)KBT–(x)BT (x = 0.25, 0.30 and 0.35) with perovskite structure were synthesised using a conventional solid-state reaction process. The first materials were the following precursor powders: pure BT powder was prepared in parallel from $BaCO_3$ (Alfa Chemika, India > 99% purity) and TiO_2 (A-HR, Huntsman, UK > 99% purity). The raw materials for the mixed ceramic were weighed and then mixed as powders, depending on the stoichiometry of the composition. The raw materials were placed in a grinding vessel, then subjected to a spherical grinding process that lasted for 24 hours, using propan-2-ol as a suspension solution, and balls of yttria-stabilized zirconia as a grinding medium to ensure a homogeneous and fine powder. The slurry was dried after that, and then calcined using a covered alumina crucible at 1300 ℃ for four hours. Pure KBT powder was prepared using potassium carbonate (K_2CO_3, from Lubashemi, India, with a purity of over 99.5%), bismuth oxide (Bi_2O_3, from Glentham Life Sciences Ltd., UK, with a purity of over 99%), and titanium dioxide (TiO_2, from Huntsman, UK, with a purity of 99%) as raw materials for the preparation of the compound. The combination was weighed, ball-milled, and then dried, following this calcined at 950 ℃ for four hours as described above [32]. Subsequently, the powder of calcined BT was mixed separately with KBT and two weight percent of additional bismuth oxide to compensate for any loss due to volatilization through subsequent high temperature sintering. The precise amount of excess bismuth oxide was chosen based on the results of a study on the effect of excess bismuth oxide on the KBT–BT ceramics' properties. Where 2 wt% excess Bi_2O_3 represented the optimal amount for the preparation of ceramics the present processing methods [31]. The powder that was calcined was re-ground for 24 hours, utilising the same conditions as in the previous milling process, with the aim of breaking up the solid agglomerates and achieving a further reduction in particle size [33]. The powders were dried, then mixed with a 2 wt% solution of polyethylene glycol (PEG) as a binder as well as a lubricant. After the calcination process, the powders with the binder added were crushed and rehomed, then formed into ceramic discs with a thickness of approximately 1.5 mm by uniaxial pressing at a pressure of 150 MPa for 40 seconds, using a cylindrical steel mold with a diameter of 10 mm. To prevent chemical reactions or diffusion of elements between the ceramic samples and the crucible base during the sintering process, the ceramic discs were placed on a thin layer of zirconia sand inside an alumina crucible with a lid. This procedure minimizes contamination and unwanted interfaith reactions, helping to maintain the purity of the material and the stability of its structural and functional properties. The organic part was first burned away by heating the pellets to 500 ℃ for two hours. Then they were sintered at 1100 ℃ with a heating rate of 5 ℃/min for 3 hours. The apparent density of the sintered samples was determined according to Archimedes' principle, using water as the

immersion medium, in order to assess the density of the samples after the sintering process. X-ray diffraction (XRD) phase analysis of pellets that were sintered was performed with CuKα radiation (λ = 1.54060 Å) utilising a Shimadzu XRD 6000, Japan. The detection range at room temperature was 20° to 60° with 0.0167° as the step size. The samples for XRD were crushed and milled into ceramic powders. 1200-grade SiC paper was used to grind the sintered samples to obtain smooth and parallel faces for electrical characterization. For electrical measurements, the ceramic pellets that were sintered were coated using silver paste. The painted samples were desiccated for each face in an oven at 150 °C for 30 minutes. 800, 1200, and 2500 grade SiC papers were used to grind the sintered pellets. This was followed by a polishing process using diamond paste with grain sizes of 6, 1, and 0.25 micrometres, respectively, with the aim of obtaining a highly smooth surface. Subsequently, the samples underwent chemical etching by immersing them in an etching solution consisting of 4% hydrochloric acid (HCl), 1% hydrofluoric acid (HF), and 95% distilled water for 15 seconds, in order to reveal the microstructure of the samples. SEM was utilised to investigate the microstructures of slow-cooled samples with chemically etched and gold-coated surfaces.

3. RESULT AND DISCUSSION

3.1 Density

The variation in bulk density of the sintered (1-x)KBT–(x)BT ceramic samples with various compositions (x = 0.25, 0.30, and 0.35) is shown in Figure 1. The results show that the density increased with increasing KBT ratio (0.65, 0.70, and 0.75) and then decreased slightly at higher concentrations. The increase in density is attributed to better densification during sintering, which favors better packing of particles, connectivity of grains, and reduction of porosity. The increased density observed indicates the formation of a more compact microstructure due to improved diffusion mechanisms and the effective pore removal during sintering.

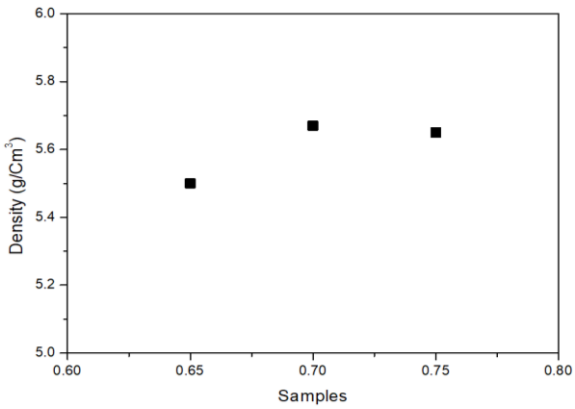


Figure 1. Illustrates the variation in the bulk density of the (1-x)$K_{0.5}Bi_{0.5}TiO_3$ (KBT)–(x)$BaTiO_3$ (BT) (x = 0.25, 0.30 and 0.35) sintered at 1100 °C for 3 h

On the other hand, the slight decrease in the higher composition ratios may be related to incomplete densification, abnormal grain growth, or the existence of residual pores that adversely influence the compactness of the ceramic structure. The results show that the composition has a great influence on densification behavior and microstructure development of KBT–BT ceramics. The optimized composition exhibits enhanced structural compactness and improved sintering properties and is suitable for advanced ceramic applications. These results are consistent with where the dielectric properties were found to increase with an increase in density [34]. Table 1 shows the densities of KBT–BT systems with various KBT content.

Table 1. Densities of KBT–BT ceramic systems

KBT Content	Absolute Density ($g.cm^{-3}$)	Theoretical Density ($g.cm^{-3}$)	Relative Density (%)
0.65	5.5	5.99	91
0.70	5.67	5.99	95
0.75	5.65	6	94

Note: KBT = $K_{0.5}Bi_{0.5}TiO_3$; BT = $BaTiO_3$.

3.2 Crystal structure

Figure 2 shows the XRD patterns of the (1-x)KBT–(x)$BaTiO_3$ ceramics with various compositions (x = 0.25, 0.30, and 0.35. XRD results showed successful perovskite phase formation in all KBT-containing samples (0.65, 0.70, and 0.75). The XRD patterns of all KBT structures indicated the presence of distinct diffraction peaks corresponding to the (100), (101), (111), (002), (200), (112), and (211) crystal planes, which are typical peaks for an ABO_3 perovskite structure, thus confirming the successful formation of the desired crystalline phase. Indicating that all ceramics display the tetragonal phase, as observed [35]. Furthermore, XRD analysis results showed that the KBT–BT ceramic samples have a tetragonal crystal structure, as evidenced by the clear splitting of the (200) and (002) reflectances into two separate and distinct peaks, which is a distinctive indicator of the presence of the tetragonal phase.

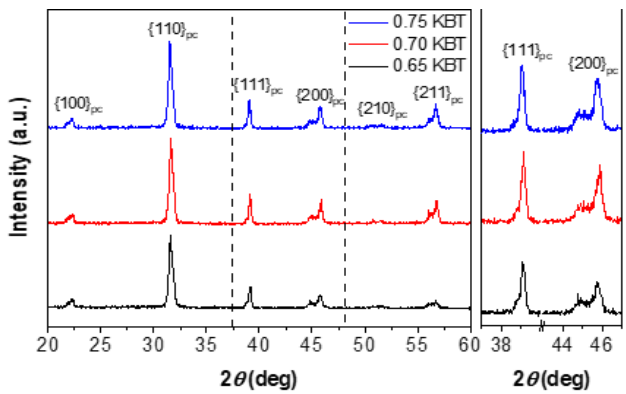


Figure 2. X-ray diffraction (XRD) patterns of the (1-x)$K_{0.5}Bi_{0.5}TiO_3$ (KBT)–(x)$BaTiO_3$ (BT) (x = 0.25, 0.30 and 0.35) sintered at 1100 °C for 3 h

3.3 Microstructure

The microstructure of the sintered (1-x)KBT–(x)BT ceramics with several compositions (x = 0.25, 0.30 and 0.35) was studied utilising SEM to evaluate the grain morphology, densification behavior, and homogeneity. In Figure 3, the SEM observations reveal a dense microstructure consisting of well-developed grains with relatively good intergranular connectivity, indicating that the sintering process effectively promoted particle bonding and mass transport mechanisms.

Figure 3(A)-(C) shows that the samples after the calcination process suffer from chemical heterogeneity, which appears as a distinct core-shell structure, separate and clear. Other studies have indicated that this microscopic structure is due to the presence of an outer shell rich in KBT material with a pseudo-cubic structure and ferroelectric properties, and inner cores with a tetragonal structure and ferroelectric properties [28].

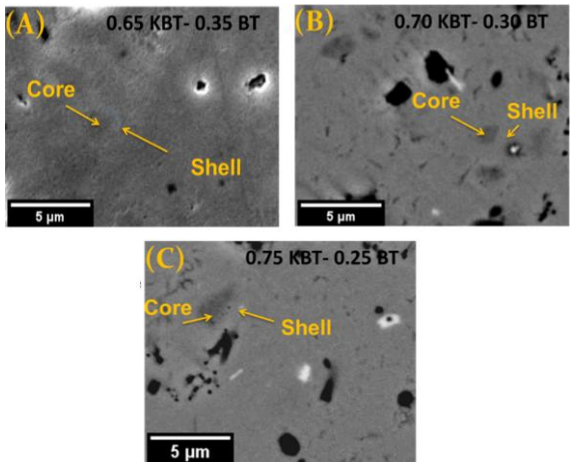


Figure 3. Scanning electron microscopy (SEM) images, captured using a backscattered electron (BSE) detector, show the surface morphology of the samples after chemical etching: (A) $0.65K_{0.5}Bi_{0.5}TiO_3$ (KBT)–$0.35BaTiO_3$ (BT), (B) 0.70KBT–0.30BT, and (C) 0.75KBT–0.25BT ceramics

The micrograph also shows a significant reduction in the pore concentration, indicating better densification during the sintering. Only a small residual porosity is observed, indicating efficient diffusion and grain rearrangement mechanisms at elevated temperatures. The dense microstructure is valuable for the improvement of dielectric and ferroelectric properties since pores are usually defect centers that reduce the efficiency of polarization. It is expected that the existence of a core–shell microstructure will be of crucial importance in the control of the functional behavior of the KBT–BT ceramic system for all KBT compositions, in agreement with previous research [33]. Therefore, the observed microstructure may be responsible for enhanced dielectric stability and improved ferroelectric response. In summary, SEM analysis indicates that a dense ceramic microstructure with distinct core–shell features was successfully achieved after the sintering process.

The BSE images shown in Figure 4 reveal a clear contrast in color variation within the ceramic granules. Darker regions appear at the granule centers due to their lower average atomic number. The accompanying elemental maps confirm that these regions are relatively rich in barium and represent the granule cores, while bismuth and potassium are more concentrated in the brighter peripheral regions. This heterogeneous elemental distribution is suggestive evidence of compositional segregation consistent with a core-shell-like microstructure with a chemically graded composition within the granules. These results indicate that the separate calcination of KBT and BT compounds contributes to the formation of a core-shell microstructure, where the core is rich in the BT phase, while the outer shell is rich in the KBT phase. The formation of the core-shell structure can be explained by the assumption that the solid BT solution exists as larger, less reactive particles, thus acting as the nucleus during the sintering process. Simultaneously, the relatively high reactivity of the KBT phase contributes to the precipitation of its components around these nuclei, forming an outer shell. This difference in kinetic and reactive behavior between the two phases results in a heterogeneous microstructure consisting of a core and shell with different chemical compositions [17, 22].

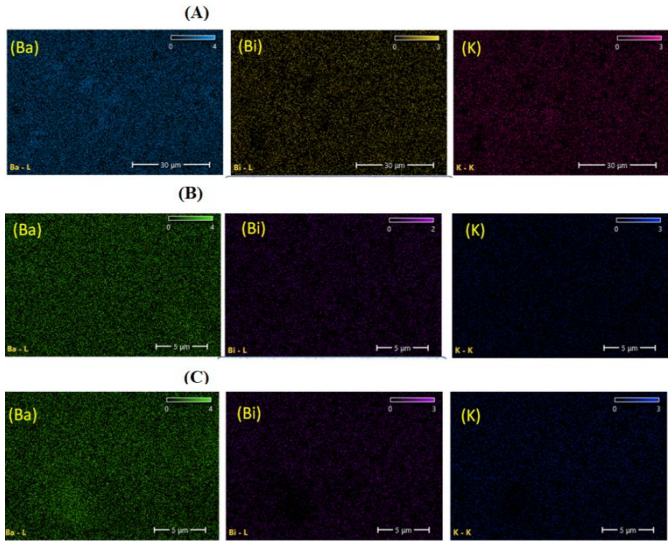


Figure 4. Scanning electron microscopy (SEM), energy-dispersive X-ray spectroscopy (EDX) elemental mapping results for (A) $0.65K_{0.5}Bi_{0.5}TiO_3$ (KBT)–$0.35BaTiO_3$ (BT), (B) 0.70KBT–0.30BT, and (C) 0.75KBT–0.25BT samples

3.4 Dielectric properties

Figures 5 and 6 show that both the dielectric constant and the dielectric loss depend on frequency, respectively, of the (1-x)KBT–(x)BT ceramics with different compositions (x = 0.25, 0.30 and 0.35). The results show that the dielectric constant gradually decreases with increasing KBT content across the studied frequency range (40 Hz – 8 MHz), while a significant increase in dielectric loss is observed with increasing KBT content within the same frequency range. This behavior reflects the change in internal polarization mechanisms and the increase in losses associated with dielectric relaxation processes within the material. This phenomenon is attributed to intergranular polarization, as the KBT compound can be deposited at the grain boundaries, which limits the movement of free charges and leads to their accumulation in the intergranular regions, resulting in the formation of intergranular polarization caused by the accumulation of charges or ions at those boundaries.

Furthermore, increasing the KBT content can weaken spontaneous polarization due to inhibited grain growth, as the grain size of the BT ceramic plays a crucial role in determining the dielectric constant. The results also indicate a decrease in the dielectric constant and a significant increase in dielectric loss with increasing frequency.

The high dielectric constant at low frequencies is explained by the involvement of all polarization mechanisms (electronic, ionic, dipole, and grain boundary polarization) in the material's dielectric response. At high frequencies, however, the limited response of some of these mechanisms to rapid changes in the alternating electric field leads to a decrease in their effective contribution, and consequently, a decrease in the overall value of the dielectric constant [36, 37]. Since electronic polarization is the dominant mechanism at high frequencies, other

polarizations such as ionic, dipole, and surface polarization contribute to the value of the dielectric constant at room temperature, but they cannot keep up with the rapid change in the electric field at high frequencies; therefore, the value of the dielectric constant decreases with increasing frequency. It is also noted that the dielectric loss is relatively low at low frequencies, which is consistent with the behavior of the dielectric constant in this frequency range.

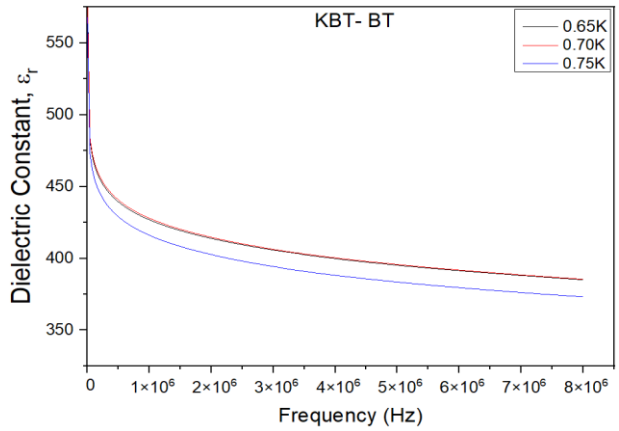


Figure 5. The relation between the frequency and dielectric constant of the (1-x)$K_{0.5}Bi_{0.5}TiO_3$ (KBT)–(x)$BaTiO_3$ (BT) ceramics with several contents (x = 0.25, 0.30 and 0.35) (KBT = 0.65, 0.70 and 0.75)

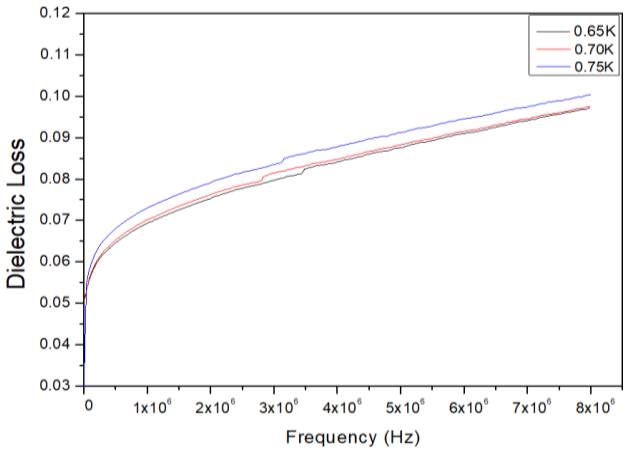


Figure 6. The relation between the frequency and dielectric loss of the (1-x)$K_{0.5}Bi_{0.5}TiO_3$ (KBT)–(x)$BaTiO_3$ (BT) ceramics with several contents (x = 0.25, 0.30 and 0.35) (KBT = 0.65, 0.70 and 0.75)

4. CONCLUSION

•XRD results showed the formation of stable perovskite phases with excellent phase compatibility, indicating successful sintering and sufficient heat treatment for the diffusion and integration of the system components.

•SEM images revealed the formation of a core-shell microstructure in all KBT–BT compositions due to interfacial diffusion and element redistribution during sintering.

•Density measurements showed that all KBT–BT ceramic samples had relatively similar densities, indicating the integrity of the microstructure and improved sintering.

•Insulator measurements showed that the KBT–BT system possessed good dielectric response, attributed to the interfacial polarization effect, the contribution of grain boundaries, and the role of the core-shell structure in enhancing the electrical properties.

•The dielectric constant was observed to decrease gradually with increasing KBT content within the frequency range (40 Hz – 8 MHz). Dielectric loss increased progressively with increasing KBT content across the same frequency range. This is attributed to the structural and microscopic changes associated with increasing KBT content and the resulting alterations in internal polarization mechanisms.

•The results confirmed that the synergistic interaction between the KBT and BT phases may contribute to the observed dielectric behavior of the composite system.

•The study demonstrated the feasibility of using the established fabrication method to produce lead-free KBT–BT ceramics with a controllable core-shell structure and superior functional properties.

ACKNOWLEDGMENT

I extend my sincere thanks and appreciation to the College of Materials Engineering – Department of Ceramics and Building Materials Engineering, University of Babylon, for providing a supportive academic environment that contributed to the completion of this study. I also express my deep gratitude to my supervisor, Assistant Professor Dr. Mohammed N. Al-Araji, for his rigorous academic supervision.

REFERENCES

[1] Noheda, B., Cox, D.E., Shirane, G., Gonzalo, J.A., Cross, L.E., Park, S. (1999). A monoclinic ferroelectric phase in the $Pb(Zr_{1-x}Ti_x)O_3$ solid solution. Applied Physics Letters, 74(14): 2059-2061. https://doi.org/10.1063/1.123756

[2] Zhang, S., Li, F., Jiang, X., Kim, J., Luo, J., Geng, X. (2015). Advantages and challenges of relaxor-$PbTiO_3$ ferroelectric crystals for electroacoustic transducers–A review. Progress in Materials Science, 68: 1-66. https://doi.org/10.1016/j.pmatsci.2014.10.002

[3] Haertling, G.H. (1999). Ferroelectric ceramics: History and technology. Journal of the American Ceramic Society, 82(4): 797-818. https://doi.org/10.1111/j.1151-2916.1999.tb01840.x

[4] Chao, X., Yang, Z., Chang, Y., Dong, M. (2009). Temperature dependence piezoelectric properties of low temperature sintered PZT–PFW–PMN ceramics with additive $LiSbO_3$. Journal of Alloys and Compounds, 477(1-2): 243-249. https://doi.org/10.1016/j.jallcom.2008.10.096

[5] Vuong, L.D., Gio, P.D. (2020). Enhancement in dielectric, ferroelectric, and piezoelectric properties of $BaTiO_3$-modified $Bi_{0.5}(Na_{0.4}K_{0.1})TiO_3$ lead-free ceramics. Journal of Alloys and Compounds, 817: 152790. https://doi.org/10.1016/j.jallcom.2019.152790

[6] Wu, J. (2020). Perovskite lead-free piezoelectric ceramics. Journal of Applied Physics, 127(19): 1-13. https://doi.org/10.1063/5.0006261

[7] Ahmed Althumairi, N., Hjiri, M., Aldukhayel, A.M., Jbeli, A., Nassar, K.I. (2025). Recent advances in dielectric and ferroelectric behavior of ceramic

nanocomposites: Structure property relationships and processing strategies. Nanomaterials, 15(17): 1329. https://doi.org/10.3390/nano15171329

[8] Vuong, L.D., Truong-Tho, N. (2017). Effect of ZnO nanoparticles on the sintering behavior and physical properties of $Bi_{0.5}(Na_{0.8}K_{0.2})_{0.5}TiO_3$ lead-free ceramics. Journal of Electronic Materials, 46(11): 6395-6402. https://doi.org/10.1007/s11664-017-5665-8

[9] Gio, P.D., Viet, H.Q., Vuong, L.D. (2018). Low-temperature sintering of $0.96(K_{0.5}Na_{0.5})NbO_3$-$0.04LiNbO_3$ lead-free piezoelectric ceramics modified with CuO. International Journal of Materials Research, 109(11): 1071-1076. https://doi.org/10.3139/146.111706

[10] Zhu, L.F., Liu, D., Shi, X., et al. (2025). Ultrahigh piezoelectric performances of (K,Na)NbO_3 based ceramics enabled by structural flexibility and grain orientation. Nature Communications, 16(1): 901. https://doi.org/10.1038/s41467-025-56074-8

[11] Czaja, P., Szostak, E., Hetmańczyk, J., et al. (2024). Thermal stability and non-linear optical and dielectric properties of lead-free $K_{0.5}Bi_{0.5}TiO_3$ ceramics. Materials, 17(9): 2089. https://doi.org/10.3390/ma17092089

[12] Zhang, X., Cui, B., Qiu, Y., Ma, R., Fan, Y. (2023). Comprehensive temperature-stable energy storage performance in core-shell structural $Na_{0.5}Bi_{0.5}TiO_3$@SrSn0.1Ti0.9O_3-(Bi_2O_3-B_2O_3-SiO_2) composites via morphology engineering. Materials Research Bulletin, 165: 112324. https://doi.org/10.1016/j.materresbull.2023.112324

[13] Xue, G., Zhou, X., Su, Y., Tang, L., Zou, J., Zhang, D. (2023). Core-shell structure and domain engineering in $Bi_{0.5}Na_{0.5}TiO_3$-based ceramics with enhanced dielectric and energy storage performance. Journal of Materiomics, 9(5): 855-866. https://doi.org/10.1016/j.jmat.2023.02.008

[14] Acosta, M., Jo, W., Rödel, J. (2014). Temperature-and frequency-dependent properties of the $0.75Bi_{1/2}Na_{1/2}TiO_3$-$0.25SrTiO_3$ lead-free incipient piezoceramic. Journal of the American Ceramic Society, 97(6): 1937-1943. https://doi.org/10.1111/jace.12884

[15] Ma, C., Tan, X., Dul'Kin, E., Roth, M. (2010). Domain structure-dielectric property relationship in lead-free $(1-x)(Bi_{1/2}Na_{1/2})TiO_3$ $xBaTiO_3$ ceramics. Journal of Applied Physics, 108(10). https://doi.org/10.1063/1.3514093

[16] Sasikumar, S., Habib, M., Sivaganesh, D., Mangaiyarkkarasi, J., Saravanakumar, S., Ahmad, P. (2025). Design, microstructure, and functional properties of core-shell structured lead-free (Bi,Na)TiO_3-based ceramics. Ceramics International, 52(1): 1191-1199. https://doi.org/10.1016/j.ceramint.2025.11.425

[17] Koruza, J., Rojas, V., Molina-Luna, L., et al. (2016). Formation of the core–shell microstructure in lead-free $Bi_{1/2}Na_{1/2}TiO_3$-$SrTiO_3$ piezoceramics and its influence on the electromechanical properties. Journal of the European Ceramic Society, 36(4): 1009-1016. https://doi.org/10.1016/j.jeurceramsoc.2015.11.046

[18] Cheng, S.Y., Shieh, J., Lu, H.Y., Shen, C.Y., Tang, Y.C., Ho, N.J. (2013). Structure analysis of bismuth sodium titanate-based a-site relaxor ferroelectrics by electron diffraction. Journal of the European Ceramic Society, 33(11): 2141-2153. https://doi.org/10.1016/j.jeurceramsoc.2013.03.020

[19] Ogihara, H., Randall, C.A., Trolier-McKinstry, S. (2009). Weakly coupled relaxor behavior of $BaTiO_3$-$BiScO_3$ ceramics. Journal of the American Ceramic Society, 92(1): 110-118. https://doi.org/10.1111/j.1551-2916.2008.02798.x

[20] Calisir, I., Amirov, A.A., Kleppe, A.K., Hall, D.A. (2018). Optimisation of functional properties in lead-free $BiFeO_3$–$BaTiO_3$ ceramics through La3+ substitution strategy. Journal of Materials Chemistry A, 6(13): 5378-5397. https://doi.org/10.1039/c7ta09497c

[21] Zhao, W., Zuo, R., Fu, J., Shi, M. (2014). Large strains accompanying field-induced ergodic phase-polar ordered phase transformations in $Bi(Mg_{0.5}Ti_{0.5})O_3$–$PbTiO_3$–$(Bi_{0.5}Na_{0.5})TiO_3$ ternary system. Journal of the European Ceramic Society, 34(10): 2299-2309. https://doi.org/10.1016/j.jeurceramsoc.2014.01.040

[22] Acosta, M., Schmitt, L.A., Molina-Luna, L., et al. (2015). Core-shell lead-free piezoelectric ceramics: Current status and advanced characterization of the $Bi_{1/2}Na_{1/2}TiO_3$-$SrTiO_3$ system. Journal of the American Ceramic Society, 98(11): 3405-3422. https://doi.org/10.1111/jace.13853

[23] Al-Aaraji, M.N., Feteira, A., Thompson, S.P., Murray, C.A., Hall, D.A. (2019). Effects of quenching on phase transformations and ferroelectric properties of 0.35 BCZT-0.65 KBT ceramics. Journal of the European Ceramic Society, 39(14): 4070-4084. https://doi.org/10.1016/j.jeurceramsoc.2019.06.016

[24] Drofenik, M., Makovec, D., Zajc, I., Langhammer, H.T. (2002). Anomalous grain growth in donor-doped barium titanate with excess barium oxide. Journal of the American Ceramic Society, 85(3): 653-660. https://doi.org/10.1111/j.1151-2916.2002.tb00146.x

[25] Chu, B.J., Chen, D.R., Li, G.R., Yin, Q.R. (2002). Electrical properties of $Na_{1/2}Bi_{1/2}TiO_3$–$BaTiO_3$ ceramics. Journal of the European Ceramic Society, 22(13): 2115-2121. https://doi.org/10.1016/S0955-2219(02)00027-4

[26] Sharma, Y., Patial, P., Rana, R., Anand, V., Kumar, A., Heera, P. (2026). Synthesis and characterization of eco-friendly $K_{0.5}Bi_{0.5}TiO_3$ ceramics: Structural and optical studies. Journal of Condensed Matter, 4(1): 47-50. https://doi.org/10.61343/jcm.v4i01.205

[27] Yuan, Q., Pu, Y. (2013). Effects of $K_{0.5}Bi_{0.5}TiO_3$ addition on dielectric properties of $BaTiO_3$ ceramics. Ceramics International, 39(4): 3507-3510. https://doi.org/10.1016/j.ceramint.2012.10.174

[28] Al-Aaraji, M.N., Hall, D.A. (2018). Influence of $K_{0.5}Bi_{0.5}TiO_3$ on the structure, dielectric and ferroelectric properties of (Ba,Ca)(Zr,Ti)O_3 ceramics. Journal of the European Ceramic Society, 38(5): 2344-2352. https://doi.org/10.1016/j.jeurceramsoc.2017.12.063

[29] Zhang, S.T., Kounga, A.B., Aulbach, E., Ehrenberg, H., Rödel, J. (2007). Giant strain in lead-free piezoceramics $Bi_{0.5}Na_{0.5}TiO_3$–$BaTiO_3$–$K_{0.5}Na_{0.5}NbO_3$ system. Applied Physics Letters, 91(11). https://doi.org/10.1063/1.2783200

[30] Jo, W., Dittmer, R., Acosta, M., et al. (2012). Giant electric-field-induced strains in lead-free ceramics for actuator applications–status and perspective. Journal of Electroceramics, 29(1): 71-93. https://doi.org/10.1007/s10832-012-9742-3

[31] Al-Aaraji, M.N., Wang, B., Feteira, A., Hall, D.A. (2025). Microstructural engineering of ferroelectric and electromechanical properties in 0.65 KBT-0.35 BCZT ceramics. Materials, 18(3): 623.

https://doi.org/10.3390/ma18030623
[32] Bhardwaj, S., Kumar, S., Thakur, N. (2023). Effect of calcination temperature on structural and electrical properties of $K_{0.5}Bi_{0.5}TiO_3$ ceramics prepared by solid-state route. Bulletin of Materials Science, 46(3): 170. https://doi.org/10.1007/s12034-023-03014-1
[33] Al-Aaraji, M.N. (2018). Nanostructured Ferroelectric Ceramics and Coatings. The University of Manchester (United Kingdom). https://www.proquest.com/openview/91eb6d5690cbcc6c9ac7802aebcacdf4/1?pq-origsite=gscholar&cbl=2026366&diss=y.
[34] M'peko, J.C., Portelles, J., Rodriguez, G. (1997). Densification process of $BaTiO_3$ containing $Bi_4Ti_3O_{12}$. Journal of Materials Science Letters, 16(22): 1850-1852. https://doi.org/10.1023/A:1018541323696
[35] Shi, J., Fan, H., Liu, X., Bell, A.J. (2014). Large electrostrictive strain in $(Bi_{0.5}Na_{0.5})$ TiO_3–$BaTiO_3$–$(Sr_{0.7}Bi_{0.2})TiO_3$ solid solutions. Journal of the American Ceramic Society, 97(3): 848-853. https://doi.org/10.1111/jace.12712
[36] Shen, Z.J., Chen, W.P., Qi, J.Q., et al. (2009). Dielectric properties of barium titanate ceramics modified by SiO_2 and by BaO–SiO_2. Physica B: Condensed Matter, 404(16): 2374-2376. https://doi.org/10.1016/j.physb.2009.04.039
[37] Mishra, A.C., Sahoo, T., Srinivas, V., Thakur, A.K. (2011). Investigation of magnetoimpedance effect on electrodeposited NiFe/Cu wire using inductance spectroscopy. Physica B: Condensed Matter, 406(3): 645-651. https://doi.org/10.1016/j.physb.2010.11.070

NOMENCLATURE

BT	barium titanate, $BaTiO_3$
BSE	backscattered electron
KBT	Potassium bismuth titanate, $K_{0.5}Bi_{0.5}TiO_3$
NBT	sodium bismuth titanate, $Na_{0.5}Bi_{0.5}TiO_3$
KNN	potassium sodium niobate, $K_{0.5}Na_{0.5}NbO_3$
EDX	energy-dispersive X-ray spectroscopy
MPB	morphotropic phase boundary
PEG	polyethylene glycol
PNRs	polar nanoregions
PTCR	positive thermal resistivity coefficient
SEM	scanning electron microscopy
$SrTiO_3$	Strontium Titanate
TEM	transmission electron microscopy
XRD	X-ray diffraction
λ	X-ray wavelength
ε_r	relative dielectric permittivity
θ	diffraction angle